

Supplementary Information for

Layer-by-layer Assembly of Ruthenium (II) Complex Anion/Layered Double Hydroxide

Ordered Ultrathin Films with Polarized Luminescence

Dongpeng Yan,^a Jun Lu,^{a*} Min Wei,^{a*} Jing Ma,^b David G. Evans,^a and Xue Duan^a

^a State Key Laboratory of Chemical Resource Engineering, Beijing University of Chemical Technology, Beijing 100029, P. R. China.

^b School of chemistry and chemical engineering, Key Laboratory of Mesoscopic Chemistry of MOE, Nanjing University, Nanjing, 210093, P.R. China.

List of Contents

1. Experimental details of (Ru(dpds)₃/LDH)_n UTFs.

2. Photoluminescence spectra of [Ru(dpds)₃]⁴⁻ aqueous solution.

Fig. S1: Emission spectrum of [Ru(dpds)₃]⁴⁻ aqueous solution.

3. Structural and morphology characterization of (Ru(dpds)₃/LDH)_n UTFs.

Fig. S2: XRD profiles and the structural model for the (Ru(dpds)₃/LDH)_n UTFs.

Table S1: 2θ degree and *d* values (Å) for (Ru(dpds)₃/LDH)_n UTFs.

Fig. S3: Top view of SEM image for (Ru(dpds)₃/LDH)_n UTFs.

Fig. S4: Side view of SEM image for (Ru(dpds)₃/LDH)_n UTFs.

Table S2: Depth and thickness parameters for the UTFs with 8, 12, 20, 28 bilayers.

Fig. S5: Polarized luminescence spectra for the (Ru(dpds)₃/LDH)₂₈ UTFs.

4. Calculation details and analysis of (Ru(dpds)₃/LDH)_n system.

Fig. S6: Geometric change profiles for the pristine [Ru(dpds)₃]⁴⁻, and Ru(dpds)₃/LDH.

Fig. S7: Frontier orbital (HOMO and LUMO) profiles for the pristine [Ru(dpds)₃]⁴⁻, and Ru(dpds)₃/LDH

Fig. S8: Calculated band structure around the Fermi energy level of Ru(dpds)₃/LDH.

5. Electrochemistry measurements of Ru(dpds)₃/LDH UTFs.

Fig. S9: Cyclic voltammetry measurements of (Ru(dpds)₃/LDH)₂₈ UTFs.

1. Experimental details of $(\text{Ru}(\text{dpds})_3/\text{LDH})_n$ UTFs.

Reagents and materials: RuCl_3 and disodium 1,10-phenanthroline-4,7-diphenylsulfonate ($\text{Na}_2(\text{dpds})$) were purchased from Alfa Aesar Chemical. Co. Ltd. Analytical pure $\text{Mg}(\text{NO}_3)_2 \cdot 6\text{H}_2\text{O}$, $\text{Al}(\text{NO}_3)_3 \cdot 9\text{H}_2\text{O}$ and urea were purchased from Beijing Chemical Co. Ltd. and used without further purification.

Ultra thin film fabrication: The synthesis and purification of tetrasodium (1,10-phenanthroline-4,7-diphenylsulfonate) ruthenium(II) ($\text{Na}_4[\text{Ru}(\text{dpds})_3]$) correspond to García-Fresnadillo's work.^[1a] The process of synthesis and exfoliation of Mg-Al-LDH (Mg/Al=3:1) were similar to that described in our previous work.^[1b] 0.1 g of Mg-Al-LDH was shaken in 100 cm³ of formamide solution for 24 h to produce a colloidal suspension of exfoliated Mg-Al-LDH nanosheets. The quartz glass substrate, was first cleaned respectively in concentrated $\text{NH}_3/30\% \text{H}_2\text{O}_2$ (7:3) and concentrated H_2SO_4 for 30 min each, and then the quartz substrate was rinsed and washed thoroughly with deionic water. The substrate was dipped in a colloidal suspension (1 g dm⁻³) of LDH nanosheets for 10 min followed by washing thoroughly with water. Then the substrate was treated with a 100 mL $\text{Ru}(\text{dpds})_3$ aqueous solution (100 μM) for 10 min and the washing procedure of $\text{Ru}(\text{dpds})_3$ was the same as that for the LDH nanosheets described above. Multi-layer films of $(\text{Ru}(\text{dpds})_3/\text{LDH})_n$ were fabricated by depositing alternatively with LDH nanosheets solution and $\text{Ru}(\text{dpds})_3$ solution for n cycles. The resulting films were dried under a nitrogen gas flow for 2 min at 25 °C.

Sample characterization: The UV-vis absorption spectra were collected in the range from 190 to 800 nm on a Shimadzu U-3000 spectrophotometer, with the slit width of 1.0 nm. The photoluminescence spectra were performed on RF-5301PC fluorospectrophotometer with the excitation wavelength of 470 nm. The photoluminescence emission spectra are in the range from 550 to 690 nm, and both the excitation and emission slit are set to 3 nm. Steady-state polarized photoluminescence measurements of $(\text{Ru}(\text{dpds})_3/\text{LDH})_n$ were recorded with an Edinburgh Instruments' FLS 920 fluorospectrophotometer. X-ray diffraction patterns (XRD) of $\text{Ru}(\text{dpds})_3/\text{LDH}$ films were recorded using a Rigaku 2500VB2+PC diffractometer under the conditions: 40 kV, 50 mA, Cu K α radiation ($\lambda = 0.154056$ nm) with step-scanned in step of 0.04° (2θ) in the range from 2 to 10° using a count time of 10 s/step. The morphology of thin films was investigated by using a

scanning electron microscope (SEM Hitachi S-3500) equipped with an EDX attachment (EDX Oxford Instrument Isis 300), and the accelerating voltage applied was 20 kV. The surface roughness and thickness data were obtained by using the atomic force microscopy (AFM) software (Digital Instruments, Version 6.12). Electrochemical measurements were performed with the model 1100A electrochemical analyzer (CH Instruments), using indium tin oxide (ITO) glass as the working electrode, platinum wire as the auxiliary electrode and Ag/Ag⁺ as the reference electrode. Cyclic voltammetry (CV) studies of the Ru(dpds)₃/LDH deposited on ITO were carried out at a scan rate of 100 mV·s⁻¹ and in N,N-dimethylformamide solution containing 0.1 M of Bu₄NBF₄ as the supporting electrolyte. Using the onset electric potentials in the CV curves, the LUMO (lowest unoccupied molecular orbital) and HOMO (highest occupied molecular orbital) energy levels can be determined.

2. Photoluminescence spectra of Ru(dpds)₃ aqueous solution.

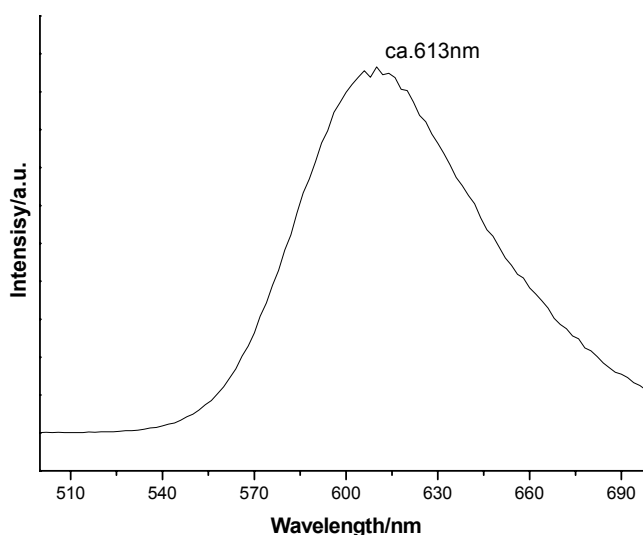


Fig. S1. Emission spectrum of Ru(dpds)₃ aqueous solution (10 μM).

3. Structural and morphology characterization of the (Ru(dpds)₃/LDH)_n UTF

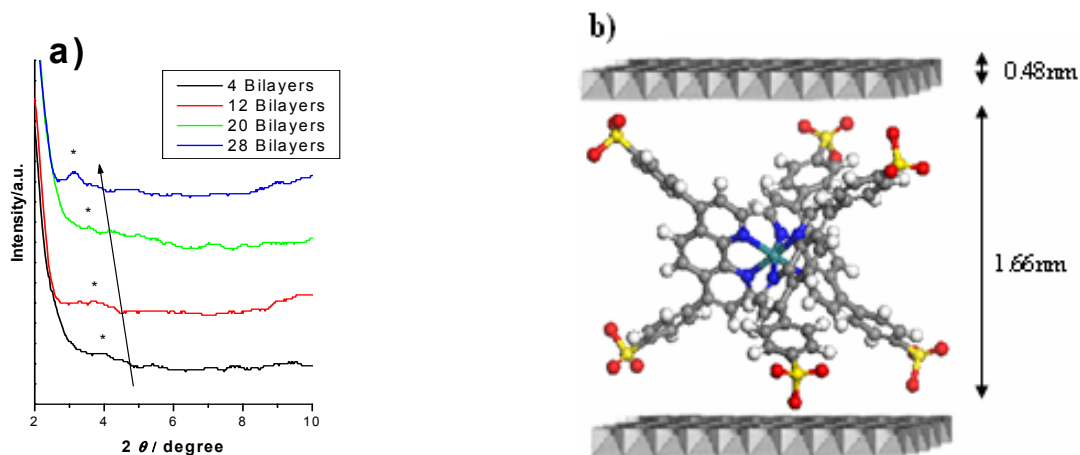


Fig. S2. (a) The small angle XRD profiles for the $(\text{Ru}(\text{dpds})_3/\text{LDH})_n$ UTFs with 4, 12, 20, 28 bilayers; (b) The structural model of $\text{Ru}(\text{dpds})_3/\text{LDH}$.

Table S1: 2θ degree and d values (\AA) for the $(\text{Ru}(\text{dpds})_3/\text{LDH})_n$ UTFs.

n	4	12	20	28
2θ (degree)	3.96	3.78	3.58	3.24
d (\AA)	22.32	23.34	24.65	27.23

The average interlayer spacing is 24.36 \AA . The derivation of the interlayer spacing of the UTFs with different bilayers may be attributed to the different stacking mode of anions. Similar phenomena was also observed in our previously work.^[1b]

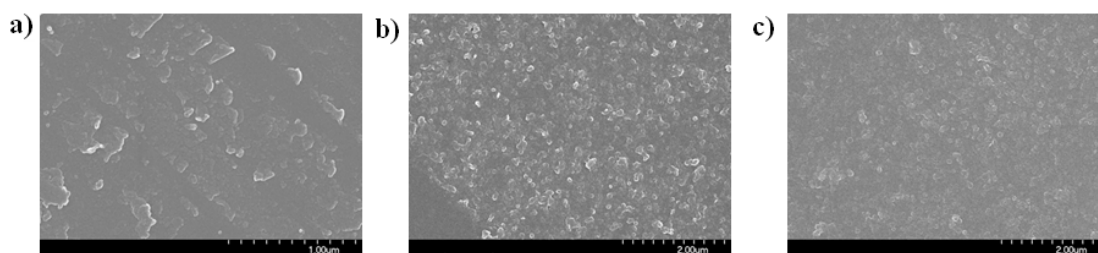


Fig. S3. The top view of SEM images for the $(\text{Ru}(\text{dpds})_3/\text{LDH})_n$ UTFs with a) 4, b) 12, c) 20 bilayers.

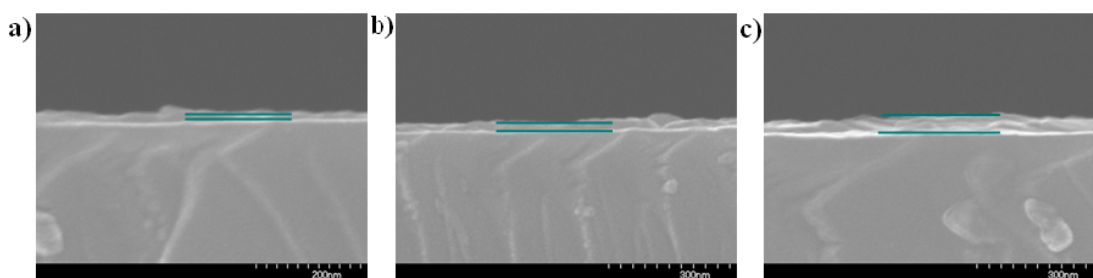


Fig. S4. The side view of SEM images for the $(\text{Ru}(\text{dpds})_3/\text{LDH})_n$ UTFs with a) 4, b) 12, c) 20 bilayers.

Table S2: Depth and thickness parameters for the UTFs with 4, 12, 20, 28 bilayers

n	4	12	20	28
rms roughness (nm)^[a]	6.813	7.780	9.138	10.646
SEM thickness (nm)^[b]	ca. 10	ca. 25	ca. 45	ca. 60

^[a] The values of statistical rms roughness were obtained by AFM.

^[b] The SEM thickness were obtained from the side view of $(\text{Ru}(\text{dpds})_3/\text{LDH})_n$ UTFs, see Fig. S4.

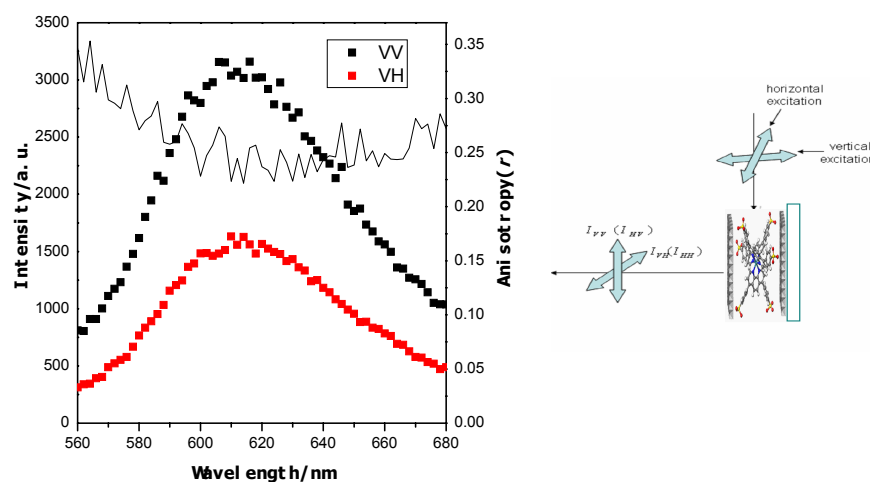


Fig. S5. Polarized luminescence profiles for the VV, VH modes and anisotropic value (r) for the $(\text{Ru}(\text{dpds})_3/\text{LDH})_{28}$ UTFs. The inset corresponds to excitation light with glancing incidence geometry as shown in the right scheme.

4. Calculation details and analysis of $(\text{Ru}(\text{dpds})_3/\text{LDH})_n$ UTFs.

4.1 Structural model of $\text{Ru}(\text{dpds})_3/\text{LDH}$: An LDH layer with R3-m space group containing 14 Mg atoms and 4 Al atoms was built. The lattice parameters of the 2-dimensional layer are $a = b = 3.05 \text{ \AA}$,

which is in accordance with other literatures.^[2] Every octahedral layer has 18 metal atoms and 36 OH groups, and a supercell was constructed with lattice parameter $a = 18.30 \text{ \AA}$, $b = 9.15 \text{ \AA}$ and the initial interlayer spacing $c = 30 \text{ \AA}$, $\alpha = \beta = 90^\circ$, $\gamma = 120^\circ$ (equivalent to a $6 \times 3 \times 1$ super cell). The supercell was treated as P1 symmetry, to which 3-dimensional periodic boundary condition was applied. Then, the representative of anionic $[\text{Ru}(\text{dpds})_3]^{4-}$ with four negative charges, were introduced into the simulated supercell to ensure the system electroneutral. As a result, the formula of the simulated structures can be expressed as: $\text{Mg}_{14}\text{Al}_4(\text{OH})_{36}(\text{RuC}_{72}\text{H}_{42}\text{O}_{18}\text{S}_6)$.

4.2 Computational method: All calculations were performed with the periodic density functional theory (DFT) method using Dmol3^[3a,b] module in Material Studio software package.^[3c] The initial configuration was first fully optimized with fixed positions for the atoms in the layer by classical molecular mechanics method employed cff91 force field,^[3d,e,f] then further optimization was implemented by Perdew-Wang (PW91)^[3g] generalized gradient approximation (GGA) method with the double numerical basis sets plus polarization function (DNP). The core electrons for metals were treated by effective core potentials (ECP). SCF converged criterion was within 1.0×10^{-5} hartree/atom and converged criterion of structure optimization was 1.0×10^{-3} hartree/bohr. The Brillouin zone is sampled by $1 \times 1 \times 1$ k -points, and test calculations reveal that increasing k -points does not affect the results.

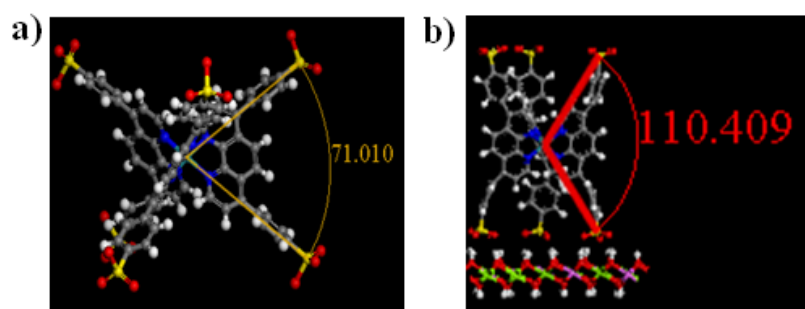


Fig. S6. Geometric profiles for a) the pristine $[\text{Ru}(\text{dpds})_3]^{4-}$ and b) $\text{Ru}(\text{dpds})_3/\text{LDH}$ assembled system.

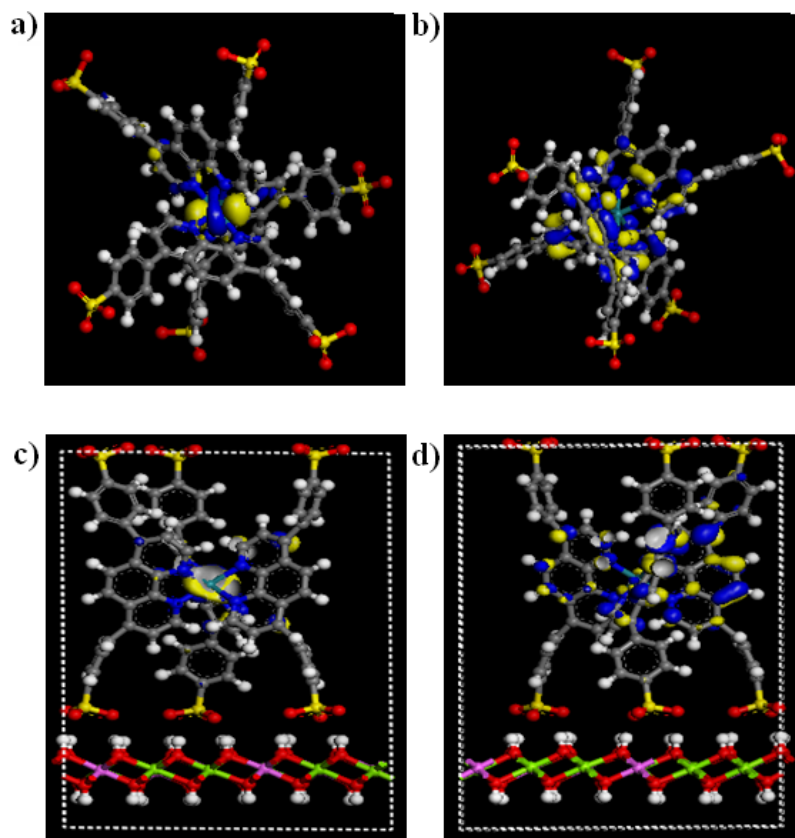


Fig. S7. a) HOMO and b) LUMO profiles for the pristine $[\text{Ru}(\text{dpds})_3]^{4+}$, c) HOMO and d) LUMO profiles for the $\text{Ru}(\text{dpds})_3/\text{LDH}$ assembled system.

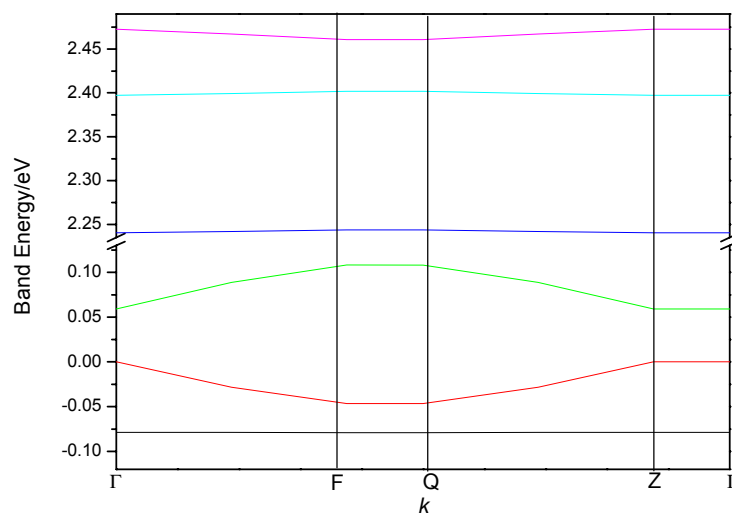


Fig. S8. a). Calculated band structure around the Fermi energy level of $\text{Ru}(\text{dpds})_3/\text{LDH}$ system. Γ (0,0,0), Z (0,0,1/2), F (0,1/2,0), and Q (1/2,0,0) are the selected reciprocal points in the first Brillouin Zone (BZ). The energy gap between conduction band (CB) and valence band (VB) at Γ point (0,0,0) in the first BZ is 2.14 eV.

The energy bands around the Fermi levels show almost complete independence on the k electron wave vectors along the ΓZ line ([001] direction), indicating the strong valence electron confinement effect on the LDH monolayer in the normal direction.

5. Electrochemistry measurements of the $(\text{Ru}(\text{dpds})_3/\text{LDH})_n$ UTFs.

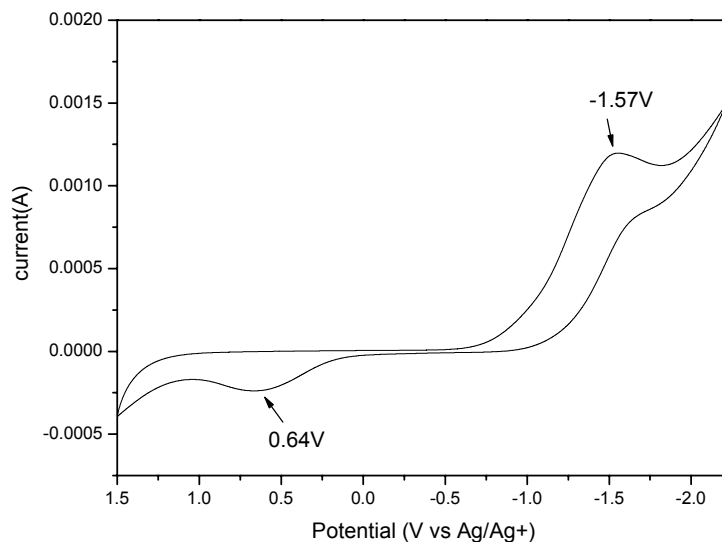


Fig. S9. Cyclic voltammogram curve of the $(\text{Ru}(\text{dpds})_3/\text{LDH})_{28}$ UTF.

Based on the empirical relationships proposed by Leeuw et al.^[4]:

$$E(\text{HOMO}) = -(E_{\text{onset,ox}} + 4.39) \text{ (eV)}$$

$$E(\text{LUMO}) = -(E_{\text{onset,red}} + 4.39) \text{ (eV)}$$

Therefore, the band gap energy can be calculated by:

$$\Delta E_g = E(\text{LUMO}) - E(\text{HOMO}) = 2.21 \text{ eV.}$$

Reference:

- [1] a) D. García-Fresnadillo, Y. Georgiadou, G. Orellana, A. M. Braun, and E. Oliveros, *Helv. Chim. Acta* 1996, **79**, 1222. b) D. P. Yan, J. Lu, M. Wei, J. B. Han, J. Ma, F. Li, D. G. Evans, and X. Duan, *Angew. Chem.Int. Ed.* 2009, **48**, 3073.
- [2] a) L. Mohanambe, and S. Vasudevan, *J. Phys. Chem. B* 2005, **109**, 15651. b) S. P. Newman, S. J. Williams, P. V. Coveney, and W. Jones, *J. Phys. Chem. B* 1998, **102**, 6710;
- [3] a) B. Delley, *J. Chem. Phys.* 1990, **92**, 508. b) B. Delley, *J. Chem. Phys.* 2000, **113**, 7756. c)

Dmol3 Module, MS Modeling, Version 2.2; Accelrys Inc.: San, Diego, CA, 2003. d) J. R. Maple, M. -J. Hwang, T. P. Stockfisch, U. Dinur, M. Waldman, C. S. Ewig, and A. T. Hagler, *J. Comput. Chem.* 1994, **15**, 162. e) D. P. Yan, J. Lu, M. Wei, H. Li, J. Ma, F. Li, D. G. Evans, and X. Duan, *J. Phys. Chem. A* 2008, **112**, 7671. f) D. P. Yan, J. Lu, M. Wei, J. Ma, D. G. Evans, and X. Duan, *Phys. Chem. Chem. Phys.* 2009, DOI: 10.1039/B907366C. g) J. P. Perdew, J. A. Chevary, S. H. Vosko, K. A. Jackson, M. R. Pederson, D. J. Singh, and C. Fiolhais, *Phys. Rev. B* 1992, **46**, 6671.

[4] D. M. de Leeuw, M. M. J. Simenon, A. R. Brown, and R. E. F. Einerhand, *Synth. Met.* 1997, **87**, 53.